



OPEN

First measurement of energy diffusion in an electron beam due to quantum fluctuations in the undulator radiation

Sergey Tomin , Evgeny Schneidmiller & Winfried Decking

Plasma and beam physics are usually considered as classical physics disciplines with quantum effects featuring only rarely. In particular, free electron lasers (FELs) even in the Angstrom regime (developed recently and being upgraded towards even shorter wavelengths) are well described by classical mechanics and electrodynamics. There is, however, a quantum effect that can influence the operation of these devices and limit the shortest achievable wavelength, namely energy diffusion in an electron beam due to quantum fluctuations in undulator radiation. Although this effect has been calculated theoretically, it has never been measured. In this paper we present measurements of quantum diffusion effect at the European X-Ray Free-Electron Laser. The method uses a recently installed wakefield structure, which enables measurements of the longitudinal phase space after the hard X-ray undulator. The effect of quantum diffusion in the undulator is measured for the first time, and the results are in good agreement with theoretical predictions.


A relativistic electron beam emits radiation while moving in magnetic fields. Consequently, its mean energy decreases and the energy spread increases due to the quantum nature of the radiation. The effect of increasing the energy spread of the electron beam due to quantum fluctuations of the radiation from bending magnets (quantum diffusion) was first described in¹. This effect mainly defines the energy spread of the beams circulating in storage rings. Quantum diffusion can also be an important effect in devices with periodic magnetic fields, namely undulators, which are widely used to produce incoherent X-ray radiation at storage rings and powerful, coherent radiation at linac-based X-ray free electron lasers (XFELs) such as the European XFEL². An importance of quantum diffusion in undulators for operation of XFELs was first pointed out in³, and the fundamental limitation on the achievement of short wavelengths in XFELs was studied in^{4,5}. The formulae describing quantum diffusion in undulators were obtained in⁶. According to those formulae, the effect increases significantly with increasing electron beam energy, undulator length and magnetic field. This is exactly what characterizes the European XFEL² which operates with electron beam energies up to 17.5 GeV and has long hard X-ray undulators such as undulators SASE1 and SASE2 (magnetic length 175 m), each with deflection parameters, K , of up to 3.9. Another feature making this effect particularly important for the European XFEL is the sequential placement of the undulators. For example, SASE1 and the soft X-ray undulator SASE3 are placed in the same electron beamline, one after the other, Fig. 1. And there is a proposal to install hard X-ray undulators after the SASE2 undulator⁷. The effect of energy diffusion can make it difficult or even impossible to operate simultaneously hard X-ray undulators in the same beamline.

The theoretical predictions of Ref.⁶ have never been cross-checked with experimental results. The above mentioned properties of the European XFEL (high electron energy, long undulators) provide a unique opportunity for such measurements. They become possible after installation of a new longitudinal phase space diagnostics after the SASE2 undulator.

Results

According to⁶ the energy diffusion for a planar undulator is given by

$$\frac{d\langle(\delta\gamma)^2\rangle}{dt} = \frac{7}{15}c\lambda_c r_e \gamma^4 k_w^3 K^2 F(K) \quad (1)$$

Deutsches Elektronen-Synchrotron DESY, Notkestr. 85, 22607 Hamburg, Germany.  email: sergey.tomin@desy.de

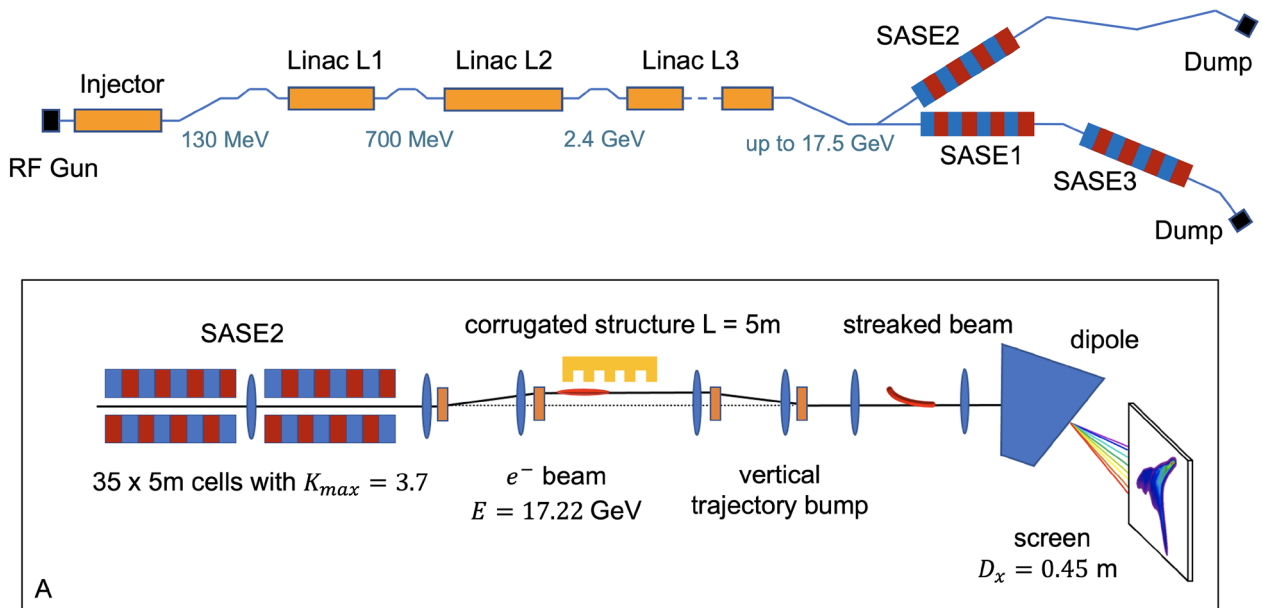


Figure 1. Simplified layout of the European XFEL from photoinjector to the electron beam dumps (not to scale). **(A)** Simplified scheme of the experimental setup for measuring quantum diffusion after the SASE2 undulator.

and

$$F(K) = 1.20K + \frac{1}{1 + 1.33K + 0.40K^2}, \quad (2)$$

where K is the undulator deflection parameter, λ_w the undulator period, r_e is classical radius of the electron, $k_w = 2\pi/\lambda_w$, and $\lambda_c = \hbar/mc$.

As can be seen from these formulae, to maximize the effect of quantum diffusion the beam energy $E = \gamma mc^2$ should be as high as possible, as well as the undulator deflection parameter K . In our measurements, the beam energy was set to 17.22 GeV, and the quantum diffusion effect came from spontaneous radiation in the SASE2 undulator, consisting of 35 cells of 5 m length each with $K_{max} = 3.7$. The simplified layout of the experimental setup is shown in Fig. 1. Beam compression was significantly reduced from the nominal 5 kA peak current to a current amplitude of about 0.5 kA. This reduces the beam slice energy spread and thus increases the measurement's accuracy. The lasing process was safely eliminated due to reduced compression in addition to an intentional trajectory perturbation inside the undulator.

We performed two experiments, firstly we measured quantum diffusion as a function of the undulator length, and secondly we measured quantum diffusion as a function of the undulator parameter K . In the first experiment the first data point was taken when all 35 cells (175 m of magnetic length) of the undulator were closed to the minimum gap corresponding to $K = 3.7$, and in each step we opened 7 undulator cells starting from the end. In the last step only the first 4 cells, corresponding to a magnetic length of 20 m, were closed. In the second experiment, where we investigated the quantum diffusion as a function of the undulator gap (or K parameter), we scanned the gap of the whole undulator, corresponding to a magnetic length 175 m, starting from the maximum at 3.7 down to the lower value of 1.6. At each measurement step we measured the slice energy spread of the electron beam.

The slice energy spread of the electron beam was measured with new a longitudinal phase space diagnostics based on a corrugated structure. In the corrugated structure the electrons are transversely deflected depending on their longitudinal position in the beam. The diagnostics consists of the corrugated structure and a screen in a down-stream dispersive section, see Fig. 1. The energy axis of the diagnostic system is calibrated by measuring the horizontal dispersion on the screen. Details about the corrugated structure and method to measure dispersion can be found in the section "Methods".

To measure the quantum diffusion effect, one must select a particular beam slice and measure the energy spread of this slice with the closed and open undulator and quadratically subtract from each other

$$\sigma_E^{\text{diff}}(K) = \sqrt{\frac{d((\delta\gamma)^2)L}{cdt}} = \sqrt{\sigma_E^{\text{slice}}(K)^2 - \sigma_E^{\text{slice}}(0)^2}, \quad (3)$$

where L is the magnetic length of the undulator, σ_E^{diff} is in mc^2 units. Note that in fact $\sigma_E^{\text{slice}}(0)$ is the convolution of energy resolution, energy spread in front of the undulator, and energy spread induced by the corrugated structure (in the following we will simply refer to $\sigma_E^{\text{slice}}(0)$ as to a slice energy spread). By quadratic subtraction we eliminate all these contributions and extract only the contribution of quantum diffusion. The distance of the electron

beam to the corrugated plate, which defines the strength of the transversal kick, was chosen so as to obtain the minimum energy spread for the selected slice while maintaining a reasonable time dependant deflection.

Let us take a detailed look at the measurement of the slice energy spread of a beam with an open undulator. It is worth noting that the magnetic field of the open undulator is negligibly small. Figure 2 shows that the region of minimum slice energy spread corresponds to the beam head, where the influence of wakefields from the corrugated structure is small, which was also shown in simulations, see “Methods”. Therefore we selected a slice corresponding to the head of the beam or the peak of the projection on the time axis. The width of the slice was chosen to be 20 px or ± 10 px with respect to the projection peak. Subsequently we obtained the energy spread for the selected slice to be $\sigma_E^{\text{slice}}(0) = 1.65$ MeV.

Finally, we obtained the energy spread of the selected slice for all measurements with a closed undulator. The quantum diffusion was calculated with Eq. (3), and the result can be seen in Fig. 3. The theoretical curves were calculated using Eq. (1). One can see very good agreement between the theory⁶ and the experiment. This is the first comparison between measurement and theory of this kind, and was only made possible thanks to the high electron energy of the European XFEL accelerator and its long variable-gap undulators.

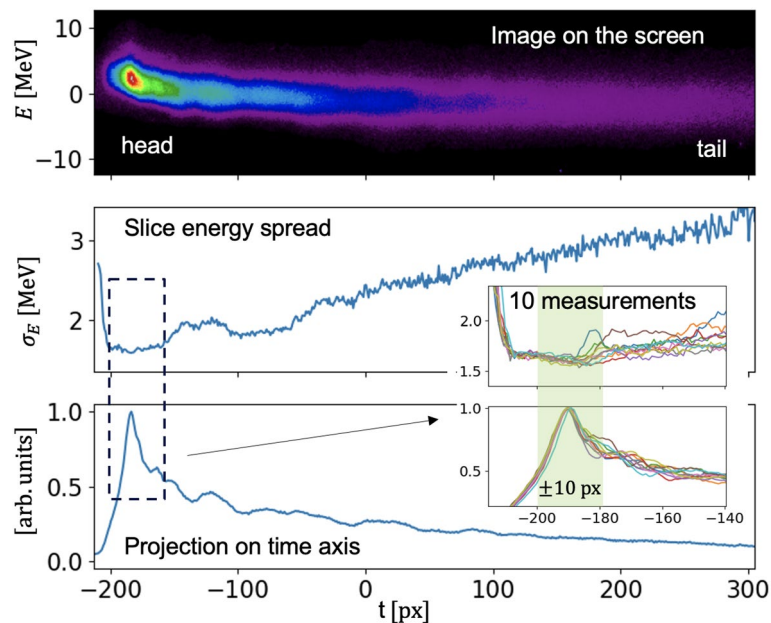


Figure 2. The beam slice energy spread measurements with the corrugated structure for the open undulator case. Zero on the time axis corresponds to the center of mass of the image.

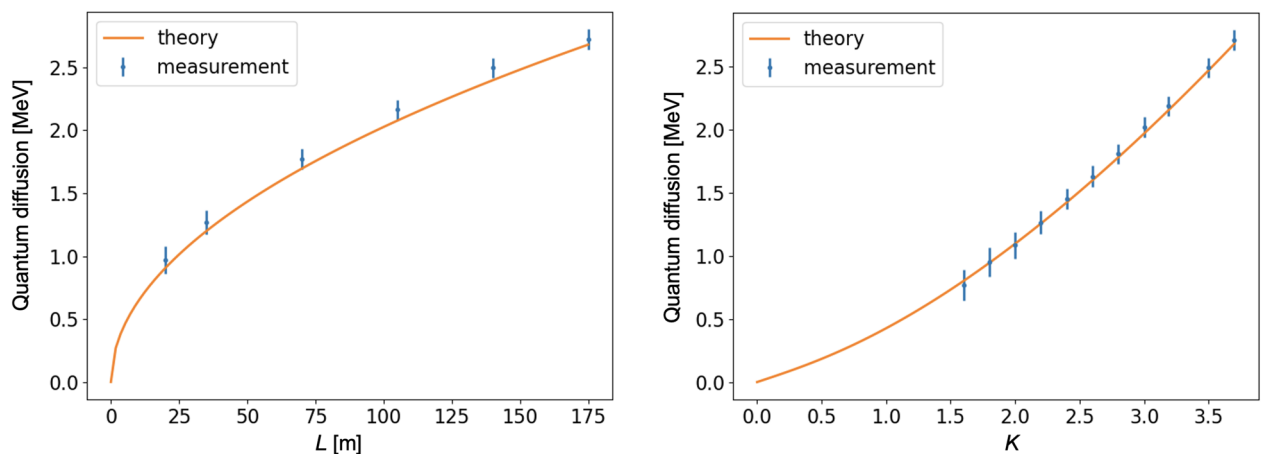


Figure 3. Left plot shows the quantum diffusion as a function of the magnetic length of the undulator for $K = 3.7$. Right picture shows the quantum diffusion as a function of the undulator deflection parameter K of the undulator with magnetic length of 175 m.

Discussion

The formula (1) was derived in⁶ assuming an ideal undulator. However, the phase error in a real undulator can distort the radiation spectrum and thus affect the diffusion process. The influence of phase error is strongest at the higher harmonics of the radiation spectrum, and it can be estimated using the results of Ref.⁸. For large K , the highest harmonic (corresponding to the critical wavelength of the synchrotron radiation) is of order K^3 , and is about 50 for the highest K value in our measurements. Using the Ref.⁸ we have estimated that the phase error effect is relatively small for hard X-ray undulators of the European XFEL with phase errors of about one degree. Moreover, for $K = 3.7$ the spectrum at high harmonics as well as the energy diffusion coefficient approach the spectrum and diffusion coefficient for synchrotron radiation, and the phase errors of the undulator no longer play a significant role.

Another effect that could potentially affect quantum diffusion measurements is photodesorption, an increase in residual gas pressure in the undulator vacuum chamber due to synchrotron radiation. In this case, the bremsstrahlung on atoms can contribute more to the energy spread when the undulator is closed. Indeed, a small increase in the residual gas pressure is observed in the operation mode with several hundred electron bunches per second. However, the LPS measurements with the corrugated structure are performed at a lower repetition rate of only 3 bunches per second, which is insufficient to change the residual gas pressure due to photodesorption. Thus, this effect can be completely neglected.

Conclusion

In summary, this paper demonstrates that measurements of energy diffusion in the electron beam due to quantum fluctuations in the undulator radiation are in good agreement with theoretical predictions. The latter have never been cross-checked with experimental results. High electron beam energy, long undulators, and the recently installed corrugated structure after the undulator at the European XFEL provided a unique opportunity to conduct such an experiment. An independent verification of the energy calibration was performed by measuring the mean beam energy loss due to synchrotron radiation and comparing it with theoretical predictions. The result also agrees well with theory.

Methods

Longitudinal phase space diagnostics based on a corrugated structure. A corrugated structure—a corrugated pipe of small radius or two corrugated metal plates with an adjustable gap—has been proposed in Ref.⁹ to remove linear energy correlation (chirp) in a relativistic electron beam and first confirmed experimentally in¹⁰. When an electron beam is displaced relative to the center of the corrugated structure and passes near the corrugated wall, it experiences a time-correlated transverse kick in the direction of the wall, thus streaking the beam perpendicular to the wall. This corrugated structure property has been used in FEL scheme, namely fresh-slice technique¹¹, and for diagnostic purposes for beam length measurement^{12,13} and recently for electron beam longitudinal phase space (LPS) measurements¹⁴.

At the European XFEL, development of the LPS diagnostics project using a corrugated structure was launched in October 2020 and put into operation in January 2022¹⁵. The new diagnostics consists of a 5 m long corrugated metal plate that is installed after the SASE2 undulator and a GAGG:Ce screen installed in a down-stream arc to take LPS images of the electron beam. The strength of the corrugated plate's transverse kick depends on the beam current distribution and the distance between the beam and the corrugated plate. The corrugated structures at PSI¹⁴ and SLAC¹⁶ both use moveable jaws with appropriate mechanics to adjust the distance to the beam. However, in our diagnostic the distance between the beam and the corrugated plate is controlled with a trajectory bump. This significantly simplifies the design of the entire system. A simplified layout of the diagnostic beam line is shown in Fig. 1, where the beam energy E , horizontal dispersion in the screen position D_x , and the deflection parameter K_{max} correspond to the experiment described in this paper. To demonstrate the measurement of the longitudinal phase space of the electron beam with the corrugated structure, we modeled the entire diagnostic beam line, see “Simulation”.

Simulation. An ideal particle distribution with a Gaussian current profile was tracked using Ocelot¹⁷ through the entire diagnostic beam line (Fig. 1). The effect of a single corrugated plate on the electron beam was simulated based on the analytical approach from^{18,19}. We observed the slice beam parameters at two beamline positions, firstly in front of the corrugated structure and then in the screen (left column, Fig. 4). The corrugated structure can be seen to induce in the beam a β -mismatch, in our case most pronounced in the vertical plane, the plane of the transverse kick, an energy chirp, and a slice energy spread.

Right column of Fig. 4 shows an image of a streaked beam on the screen and the result of processing this image, see “Image analysis”. The measurement accuracy will be higher if we choose a slice with the minimum energy spread. As we can see, the slice energy spread from the image analysis has a minimum at the beam head.

Image analysis. The streaked beam image was analysed by fitting each column of pixels with a Gaussian function, where the centre of said fit corresponds with the mean slice energy and the standard deviation with the slice energy spread. The processing algorithm is the same as in the processing of real images taken during measurements as well as images obtained in simulation.

Energy calibration and resolution. To calibrate the energy axis of the diagnostic system, the horizontal dispersion at the screen position was measured by scanning the voltage of the last accelerator RF station and measuring the center of mass of the beam on the screen. The measured dispersion was $D_x = 0.454$ m.

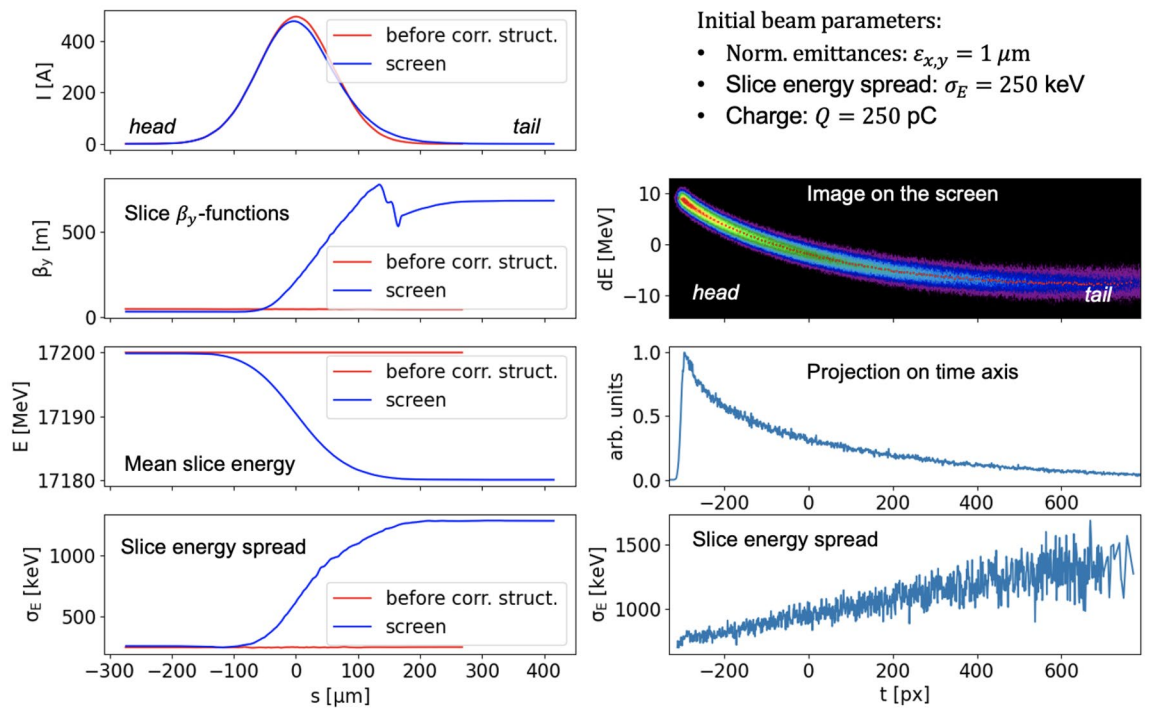


Figure 4. Modeling of the longitudinal phase space measurement with the corrugated structure. The initial beam parameters of an ideal Gaussian beam were chosen to be close to the estimated beam parameters during the quantum diffusion effect measurement. Left column shows the beam distribution before the corrugated structure and in the screen position, right column shows the image of the streaked beam and its analysis.

We independently verified the energy calibration of our diagnostic system using our obtained images. The mean energy of an electron beam decreases due to synchrotron radiation, and the analytical formula for energy losses in an undulator with length L has the form:

$$U = \frac{4\pi^2}{3} \frac{r_e E^2 K^2 L}{mc^2 \lambda_w^2} \tag{4}$$

The mean energy loss can be measured by knowing the dispersion at the position of the screen and the shift in the centre of mass of the beam image on the screen for various undulator configurations. The result is shown in Fig. 5. One can also consider this measurement in a different way. Namely, the energy loss induced in the undulator can be used for dispersion calibration. By doing this we got the following dispersion values: 0.451 m

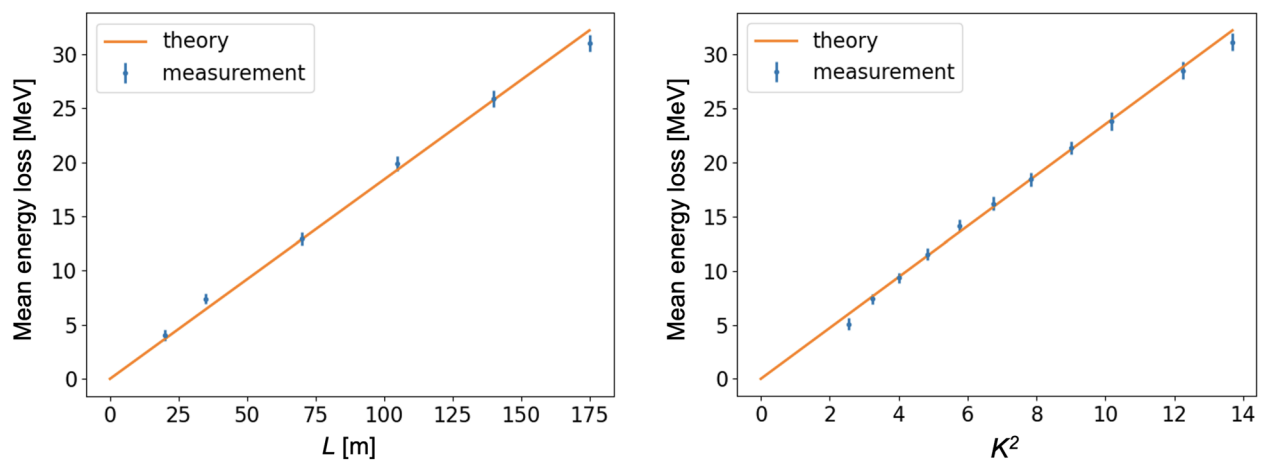


Figure 5. The mean beam energy loss due to synchrotron radiation. The left plot shows measurements of the beam energy loss for a range of undulator magnetic lengths L . The right plot shows measurements of the beam energy loss for a range of the undulator K parameters. Theoretical lines obtained with Eq. (4).

for the measurement with the undulator length and 0.450 m for the measurement with K . They are in a good agreement with the measurement using an energy change in the accelerator.

A possible effect that could affect the dispersion calibration in this way is the energy loss due to coherent radiation in the undulator²⁰. However, as was shown in²¹, this effect is strongly suppressed by the transverse size of the electron beam. Our estimates show that the energy loss due to coherent radiation is negligible for any reasonable electron beam model.

The energy resolution was also measured. The maximum resolution of 1.43 MeV corresponds to the head of the beam, and decreases toward the tail of the beam.

Data availability

The datasets used and/or analysed during the current study available from the corresponding author on reasonable request.

Received: 12 October 2022; Accepted: 24 January 2023

Published online: 28 January 2023

References

- Sands, M. Synchrotron oscillations induced by radiation fluctuations. *Phys. Rev.* **97**, 470 (1955).
- Decking, W. *et al.* A MHz-repetition-rate hard X-ray free-electron laser driven by a superconducting linear accelerator. *Nat. Photon.* **14**, 391 (2020).
- Derbenev, Ya. S., Kondratenko, A. M. & Saldin, E. L. *Nucl. Instr. Methods* **193**, 415 (1982).
- Rosbach, J., Saldin, E. L., Schneidmiller, E. A. & Yurkov, M. V. *Nucl. Instr. Methods A* **374**, 401 (1996).
- Saldin, E. L., Schneidmiller, E. A. & Yurkov, M. V. *Opt. Commun.* **235**, 415–420 (2004).
- Saldin, E. L., Schneidmiller, E. A. & Yurkov, M. V. Calculation of energy diffusion in an electron beam due to quantum fluctuations of undulator radiation. *Nucl. Instr. Methods Phys. Res. Sect. A* **381**, 545–547 (1996).
- Workshop, Shaping the Future of the European XFEL: Options for the SASE4/5 Tunnels, 6–7 December 2018. <https://indico.desy.de/event/21806/>
- Tanaka, T. Universal representation of undulator phase errors. *Phys. Rev. Accel. Beams* **21**, 110704 (2018).
- Bane, K. L. F. & Stupakov, G. Corrugated pipe as a beam dechirper. *Nucl. Instrum. Methods Phys. Res. Sect. A Accel. Spectrom. Detect. Assoc. Equip.* **690**, 106–110 (2012).
- Emma, P. *et al.* Experimental demonstration of energy-chirp control in relativistic electron bunches using a corrugated pipe. *Phys. Rev. Lett.* **112**, 034801 (2014).
- Lutman, A. A. *et al.* Fresh-slice multicolour X-ray free electron lasers. *Nat. Photon.* **10**, 745 (2016).
- Bettoni, S., Craievich, P., Lutman, A. A. & Pedrozzi, M. Temporal profile measurements of relativistic electron bunch based on wakefield generation. *Phys. Rev. Accel. Beams* **19**, 021304 (2016).
- Seok, J., Chung, M., Kang, H.-S., Min, C.-K. & Na, D. Use of a corrugated beam pipe as a passive deflector for bunch length measurements. *Phys. Rev. Accel. Beams* **21**, 022801 (2018).
- Dijkstal, Philipp *et al.* Self-synchronized and cost-effective time-resolved measurements at X-ray free-electron lasers with femto-second resolution. *Phys. Rev. Res.* **4**, 013017 (2022).
- Tomin, S. *et al.* Longitudinal phase space diagnostics with corrugated structure at the European XFEL. In *Proceedings of the 13th International Particle Accelerator Conference IPAC2022, Thailand*. <https://doi.org/10.18429/JACoW-IPAC2022-MOPOPT020> (2022).
- Guetg, M. W., *et al.* Commissioning of the RadiaBeam/SLAC dechirper. Report No. SLAC-PUB-16834, SLAC (2016).
- Agapov, I., Geloni, G., Tomin, S. & Zagorodnov, I. OCELOT: A software framework for synchrotron light source and FEL studies. *Nucl. Instr. Methods Phys. Res. A* **768**, 151–156 (2014).
- Bane, K., Stupakov, G. & Zagorodnov, I. Wakefields of a Beam near a Single Plate in a Flat Dechirper, Report No. SLAC-PUB-16881, SLAC (2016).
- Zagorodnov, I., Feng, G. & Limberg, T. Corrugated structure insertion for extending the SASE bandwidth up to 3% at the European XFEL. *Nucl. Instrum. Methods A* **837**, 69–79 (2016).
- Saldin, E. L., Schneidmiller, E. A. & Yurkov, M. V. Radiative interaction of electrons in a bunch moving in an undulator. *Nucl. Instrum. Methods A* **417**, 158–168 (1998).
- Geloni, Gianluca, Saldin, Evgeni, Schneidmiller, Evgeni & Yurkov, Mikhail. Longitudinal impedance and wake from XFEL undulators: Impact on current-enhanced SASE schemes. *Nucl. Instrum. Methods A* **583**, 228–247 (2007).

Acknowledgements

The authors thank Igor Zagorodnov, Nina Golubeva and Stuart Walker for helpful discussions and corrections. A special thank to Torsten Wohlenberg for the fast construction of the corrugated structure. We thank members of DESY's European XFEL team for providing help and the conditions to carry out the measurements.

Author contributions

Measurements: S.T. and E.S. Data analysis: S.T. Diagnostics development: W.D. and S.T. Writing—review and editing: all authors.

Funding

Open Access funding enabled and organized by Projekt DEAL.

Competing interests

The authors declare no competing interests.

Additional information

Correspondence and requests for materials should be addressed to S.T.

Reprints and permissions information is available at www.nature.com/reprints.

Publisher's note Springer Nature remains neutral with regard to jurisdictional claims in published maps and institutional affiliations.



Open Access This article is licensed under a Creative Commons Attribution 4.0 International License, which permits use, sharing, adaptation, distribution and reproduction in any medium or format, as long as you give appropriate credit to the original author(s) and the source, provide a link to the Creative Commons licence, and indicate if changes were made. The images or other third party material in this article are included in the article's Creative Commons licence, unless indicated otherwise in a credit line to the material. If material is not included in the article's Creative Commons licence and your intended use is not permitted by statutory regulation or exceeds the permitted use, you will need to obtain permission directly from the copyright holder. To view a copy of this licence, visit <http://creativecommons.org/licenses/by/4.0/>.

© The Author(s) 2023